EE

GSI

GSI-Preprint-96-63
Dezember 1996

RECENT DEVELOPMENTS AT THE GSI ON-LINE MASS SEPARATOR

K. Burkard, R. Collatz, M. Hellström, Z. Hu, W. Hüller, O. Klepper, R. Kirchner, E. Roeckl, K. Schmidt, M. Shibata, A. Weber

COUPLING A TOTAL ABSORPTION SPECTROMETER TO THE GSI ON-LINE MASS SEPARATOR

M. Karny, J.M. Nitschke, L.F. Archambault, K. Burkard, D. Cano-Ott, M. Hellström, W. Hüller, R. Kirchner, S. Lewandowski, E. Roeckl, A. Sulik

RELEASE STUDIES OF ELEMENTARY AND METAL-FLUORIDE IONS AT THE GSI ON-LINE MASS SEPARATOR

R. Kirchner

Contributions to 13th Int. Conf. on Electromagnetic Isotope Separators and Techniques Related to their Applications (EMIS-13), Bad Dürkheim, 22-27 September 1996,

(to be published in Nuclear Instruments and Methods in Physics Research, Section B)

Gesellschaft für Schwerionenforschung mbH
Planckstraße 1 • D-64291 Darmstadt • Germany
Postfach 11 05 52 • D-64220 Darmstadt • Germany

Release studies of elementary and metal-fluoride ions at the GSI on-line mass separator

R. Kirchner

GSI Darmstadt, Planckstrasse 1, D-64291 Darmstadt, Germany

Abstract

By using the techniques of *implantation of heavy ions* and of *bunched-beam release* at the GSI on-line mass separator systematic release studies were performed. With the first technique the complete release process from the catcher-ionsource-system is analyzed in detail for 31 new tracer-host combinations. These include as new tracers the elements Ti, V, Zn, Sb, and Dy, and carbon foils of around 1 mg/cm^2 thickness as new catcher matrix. The carbon foils allow for a more reliable determination of tracer diffusion properties in carbon, avoiding the problems with porous sinter-graphites, where closed pores, inconsistencies in the manufacturer's data on grain size, or grain growth cause unacceptably large discrepancies within the derived diffusion coefficients.

Measured with the bunched-beam-release technique, the mean adsorption times of fluoride-ions of group IIA and IIIA metals turned out to be orders of magnitude shorter than for the respective metal ions, thus showing quantitatively the benefits of the CF_4-fluorination technique. The degree to which the respective alkali-fluoride ions are suppressed was determined to be $< 10^{-5}$, compatible with zero. The degree of fluorination is high in most cases, even for very low CF_4 partial pressures.

1. Introduction

The catcher-ion-source-system (CISS) of the GSI on-line mass separator comes close to the principally simplest CISS: i.e. a box with a hole representing the ion source, in which a piece of solid state material acts as catcher. This structural simplicity allows for a very detailed analysis of measured release profiles, yielding basic data on solid state diffusion and surface adsorption [1]. Vice versa the knowledge of diffusion coefficients, mean surface sticking times (or the heat of desorption), and of ionization efficiencies for a certain element readily permits the calculation of the halflife-dependent separation efficiency for a certain isotope. Both options were utilized for this study.

Chapter 2 describes the release characteristics of various tracer/host combinations, obtained by simulating the implantation of (radioactive) reaction products by the implantion of stable-isotope beams from the heavy-ion accelerator UNILAC into the CISS [1]. Some of the measured release profiles or the resulting separation efficiencies are presented in chapter 2, together with a compilation of all the derived data on solid state diffusion, desorption, and on the ionization efficiency.

In chapter 3 the halflife-dependence of the separation efficiency for Ba^+ and BaF^+ ions is deduced, using both material constants from literature and desorption data determined within this work, especially the mean sticking times times for alkaline-earth fluorides. Since the on-line investigation of the very neutron-deficient isotopes $^{114-118}Ba$ required a very selective separation technique, the separation power of the CF_4-fluorination method [2] was quantitatively investigated with respect to both the degree of fluorination of group IIA and IIIa metals and the suppression of contaminations in the fluoride sideband.

2. Release profiles and derived data

Previous investigations [1] have shown that the calibration of the separation efficiency of the GSI on-line mass separator is most effectively performed, implanting primary beam particles from the UNILAC into the CISS and measuring the time dependence of their release. Since the rate of the implanted particles is known, and since the release profile is in general unambiguously determined by diffusion in the solid-state catcher and by effusion (molecular flow plus multiple ad/desorption) in the gas phase, a proper analyis yields the parameters that are decisive for an efficient release of short-lived isotopes from the CISS: the ionization efficiency η_i from the saturation value of the release profile, and from its slope the delay parameters μ_o and ν for diffusion and effusion, respectively.

The extraction of mean sticking times from ν-data is not always possible, since for this purpose the CISS should have essentially only one clearly defined wall material and temperature. Also the sticking times have to be within certain limits, i.e. sufficiently long to compete with the mean flight times between two wall collisions, but not so long that re-diffusion becomes a process competitive to desorption. In the latter case the analysis is not only doubtful with respect to ν but also to μ_o.

Another problem is associated with catchers of thin lathed sintergraphite disks, where the analysis yields diffusion coefficients which are inconsistent with the manufacturer's data on grain sizes; see ref. [1] and table 1, in which all analyzed data are compiled. To avoid systematic errors caused by the complex structure of porous sintergraphites, in new measurements also the release from graphite foils of 1 mg/cm^2 (≈ 5μm) thickness was investigated, since here the matrix is clearly defined. The measured release profiles are shown in fig. 1, yielding the unexpected result that the release from the 5 μm-foils of is much faster than from the sintergraphite disks. If one considers the latter as an ensemble of spheres of ≈ 4 μm diameter, one should expect just the opposite: spheres are faster diffusion matrices than foils of similar linear dimensions [8], and the rugged sinterdisks allowed for a higher operation temperature than the very sensitive foils. The assumption of an additional surface delay in the maze of the open porosity does, however, not reconcile with the extremely fast release of silver, especially since Ag sticks more strongly to graphite-surfaces [1] than Zn, Kr, Xe, or Pb. More plausible explanations seem to be (i) larger grain sizes than stated by the manufacturers or grain growth, and (ii) trapping in closed pores which explained why noble gases are delayed most. The escape from a closed pocket requires re-diffusion into the solid state which is least likely for tracers that do stick least to surfaces. Independent of the reason, the experimental results suggest to treat solid state diffusion coefficients with caution (including the ones presented in table 1 and ref. 1), if evaluated from measurements at porous sintermaterials.

In fig. 2 the release of some more refractory elements from a discharge ion source with graphite electrodes is presented, showing for antimony that surface delays can to some extent be reduced by a coating of pyrolytic graphite. Fig. 3 gives the release profiles for various elements with ionization potentials that are sufficiently low to allow for efficient thermo-ionization in hot cavities. Here rhenium-surfaces yield the higher ionization efficiencies, while tantalum catchers yield the faster release. This suggests the use of tantalum catchers in a rhenium enclosure which is usually the optimum solution, even though the gradual poisoning of the ionizing surfaces by tantalum vapour causes a decrease in separation efficiency by a factor of typically 3 within 12-16 hours.

3. Characteristics of fluoride ions

Our investigation of the very neutron-deficient isotopes $^{114-118}$Ba [9] required - due to low production rates and unspecific or rare decay modes (exception ^{117}Ba) in presence of much more abundantly produced contaminations - a very selective separation process. The best option is thermoionization of BaF molecular ions: it is known to suppress all contaminations including the alkali elements very strongly [10], the fluorination can be effectively performed on-line by adding small quantities of CF_4 into the ionizer [2], and the thermoionization of BaF molecules is very efficient even at relatively moderate temperatures [11]. Although well-established [2, 10-13], literature data for the CF_4 method are mostly of qualitative nature, giving e.g. no quantitative answers to the questions:

(i) to what extent does fluorination and to what extent does ionization determine the ratio of BaF^+/Ba^+?
(ii) How quantitatively (and why?) is Cs suppressed in the fluoride sideband?
(iii) Could the mass separation of BaF^+ be obscured by BaO^+ ions, as reported [14] to be formed with the residual oxygen vapour pressure?

In order to find the answers, the ratios of molecular-ion/metal-ion currents were determined for both thermoionization and electron impact ionization. Since the latter is not very sensitive to the ionization potential, the effects of ionization and fluorination can be separated. The results of the detailed investigations, performed off-line and extended to other elements of group IA-IIIA, available as trace elements within the ionic background of the applied ion sources, are compiled in table 2.

Demonstrating clearly the separation power of the CF_4 technique, all measured *alkali-fluoride/alkali* (also *BaO/Ba*) current ratios are close too and compatible with zero. This is neither due to insufficient fluorination, nor (at least not solely) due to low thermo-ionization efficiency of the fluorides, since these ratios are also practically zero when introducing alkali-fluoride vapour, or when ionizing with 150 eV electrons. Also thermal dissociation of the alkali-fluoride molecules to such a high degree is excluded by dissociation energies of 5 to 6 eV [15], leaving as explanation only that the loss of a binding electron in the ionization process causes instant dissociation.

For all tabulated elements of *group IIa* and *group IIIa* the degree of fluorination is sufficient already at low CF_4 flows and may be increased by higher flows. Barium very easily converts into the fluoride and the thermo-ionization efficiency of BaF is widely independent of the CF_4 flow in the range from 4×10^{-7} to 10^{-4} std. cm^3/s, the BaF^+/Ba^+ ratio increasing from ≈6 to ≈400 within this range. For some of the fluorides thermo-ionization is excluded due to too high ionization potential; a satisfactorily selective and efficient separation may still be achieved by the intrinsicly less selective ionization in a gaseous discharge.

A further open question was the halflife dependence of the separation efficiency for both Ba and BaF, the knowledge of which was essential for the determination of the $^{114-118}Ba$ production cross-sections [9], and especially of the branching ratio of the expected ^{12}C-cluster decay of ^{114}Ba [16]. Even though perfectly suited for these measurements, the implantation technique described in the previous chapter could not be applied, since no barium beam was available from the UNILAC.

This was no problem for the release of barium from the high temperature cavity ion source (upper curve in fig. 4), since here all decisive parameters are known: at the operation temperature of 2700 K the ionization efficiency is close to 100% [4], the mean adsorption time around 100 µs [6], the mean number of wall collisions of the order of 300, and a mean time of 2 s is calculated for diffusion in the thin tantalum catchers from the known Arrhenius coefficients (D_o = 0.21 cm^2/s, E_A = 94.3 kcal/mole [3]).

For barium isotopes separated as BaF^+ ions in a special cavity (see inset in fig. 4) operated at 2400 K with CF_4, the situation was not so simple, since both ionization efficiency and mean sticking times for the fluorides were not known. The latter were determined analoguously to the measurements for metallic ions [6] with the aid of a dedicated thermoionizer incorporating a heatable cold trap (bunched-beam technique). The τ_a-values, derived from the temporal dependence of the ion currents over the cooling/heating cycle, are compiled in table 2 and show that fluorination does in all considered cases drastically reduce the wall sticking times. The slope of the BaF-curve in fig. 4 being thus fixed, its "efficiency-calibration" was enabled via the ratio of 1.6 measured on-line for the separation rates of ^{117}Ba at 2700 K and of ^{117}BaF at 2400 K, respectively. Analoguously curve c in fig. 4 was calibrated, showing that barium is a particularily favourable case, where fluorination does not only guarantee perfect selectivity and reduces the mean adsorption times considerably, but also increases the ionization efficiency, in accordance with the literature data on the ionization potentials.

Acknowledgement

I am indebted to K. Burkard and W. Hüller for their competent help in any technical respect, to the target laboratory for preparing the numerous catcher foils, and to the UNILAC operating crews for delivering the beams required for these investigations.

References

[1] R. Kirchner, Nucl. Instr. and Meth. B 70 (1992) 186.

[2] P. Hoff, L. Jakobsson, B. Johansson, P. Aagaard, G. Rudstam, and H.-U. Zwicky, Nucl. Instr. and Meth. 172 (1980) 413.

[3] G.J. Beyer, W.D. Fromm, and A.F. Novgorodov, Nucl. Instr. and Meth. 146 (1977) 419.

[4] R. Kirchner, K. Burkard, W. Hüller, and O. Klepper, Nucl. Instr. and Meth. 186 (1981) 295 and Nucl. Instr. and Meth A 292 (1990) 203.

[5] R. Kirchner, Nucl. Instr. and Meth B 26 (1987) 204, and Nucl. Instr. and Meth. A 247 (1986) 265.

[6] R. Kirchner, K. Burkard, W. Hüller, and O. Klepper, Nucl. Instr. and Meth. B 70 (1992), 56.

[7] H. Roßbach and B. Eichler, Zentralinstitut für Kernforschung, Rossendorf, Reports ZfK-527 and ZfK-560.

[8] M. Fujioka and Y. Arai, Nucl. Instr. and Meth. 186 (1981) 409.

[9] A. Guglielmetti et al. GSI Scientific Rep. 1994, GSI Rep. 95-1, p. 28, and Z. Janas et al., to be published.

[10] H.L. Ravn, S. Sundell, and L. Westgaard, Nucl. Instr. and Meth. 123 (1975) 131.

[11] Y. Kawase, K. Okano, M. Shibata, and A. Taniguchi, Nucl. Instr. and Meth. B 70 (1992) 146.

[12] C.F. Liang, P. Paris, D. Bucurescu, S. Della Negra, J. Obert, and J.C. Puteaux, Z. Phys. A 309 (1982) 185.

[13] R. Eder, H. Grawe, E. Hagebo, P. Hoff, E. Kugler, H.L. Ravn, and K. Steffensen, Nucl. Instr. and Meth. B 62 (1992) 535.

[14] M. Hellström, B. Fogelberg, L. Jacobsson, L. Spanier, and G. Rudstam, Nucl. Instr. and Meth. B 70 (1992) 142.

[15] Constants of Diatomic Molecules, eds. K.P. Huber and G. Herzberg, Van Nostrand Reinold Co., N.Y. 1979.

[16] A. Guglielmetti, R. Bonetti, G. Poli, P.B. Price, A.J. Westphal, Z. Janas, H. Keller, R. Kirchner, O. Klepper, A. Piechaczek, E. Roeckl, K. Schmidt, A. Plochocki, J. Szerypo, and B. Blank, Phys. Rev. C 52 (1995) 740.

Table 1

Compilation of diffusion and effusion data determined with the implantation technique; addendum to table 2 in ref. 1, where the experimental conditions and the analysis are described in greater detail.

Tracer: Implanted UNILAC beam particles.

Matrix: Catcher material inside the ion source. Nb, Ta, W, Re: foils of 3 µm thickness; C: foil of 1 mg/cm^2; C2-23 (C4-9): sintergraphite disks of 0.1-0.2 mm thickness with 2 (4) µm mean grain size and 23% (9%) open porosity, respectively. Diffusion coefficients for sintergraphites are of doubtful quality, see text.

E_A, D_O: Arrhenius coefficients for solid state diffusion. Values in parentheses are based on only 2 or 3 D(T) measurements and do not allow for extrapolation beyond the narrow temperature range.

D(T): Diffusion coefficient for the given temperature; error estimated to be within a factor of 1.5; error of T within $\pm$50 K. In the case of more than one diffusion process the weight of the main component is given.

$1/\mu_O$: Measure for the mean delay $\pi^2/12\mu_0$ by solid state diffusion in the catcher; base of the stated D(T) values.

Ion source or Ref. (the latter indicates data from other work, included for comparison): TIS are cavity-type thermoionizers [4] with Ta, W, or Re enclosure, respectively. Their operation temperature corresponds to the catcher temperature. FEBIAD sources are hot space-charge–compensated electron bombardment sources with Ta-cathode. Type B2 [5]: Ta-electrodes, BN-insulators, mean operation temperature 1850 K. Type E [4]: Graphite electrodes, BeO-insulators, 2200 K (E2: version formerly [1] denoted E; E4: modified version with pyrolytic graphite coating of the inner surfaces and the option of mounting thin catcher foils). Type H [6]: Ta-electrodes, no insulators within the high temperature enclosure, 2300 K.

1/ν: Mean delay due to effusion. A "*" indicates that wall sticking times are negligible and that the stated value gives the calculated molecular flow limit.

τ_a: Mean surface sticking times for the systems with unique wall materials. Derived from measured 1/ν values, dividing by the mean number of wall collisions which are around 300 for TIS and around 1000 for FEBIAD.

ΔH_a: Enthalpy of adsorption. (i) Derived from τ_a values via the known $\tau_a(\Delta H_a)$-dependence for tantalum surfaces [1, 6]; (ii) derived from bunched-beam release studies [5]; (iii) from the semi-empirical tables of Eichler et al. [7].

η_i: Ionization efficiency, determined from the saturation values of the transmission-corrected release profiles: relative error $\mp$ 15%. A ">" indicates that the profile was not measured long enough to reach saturation.

Table 1

Solid state diffusion in the catcher							Effusion and ionization in the enclosure						
Tracer	**Matrix**	**Temperature range *[K]***	**E_A *[kcal/mole]***	**log D_0 *[cm^2/s]***	**D(T[*K*]) - weight *[cm^2/s]***	**$1/\mu_0$ *[s]***	**Ion source or Ref.**	**$1/\nu$ *[s]***	**τ_a *[ms]***	**ΔH_a *[eV]***	**ΔH_a *[eV]***	**ΔH_a *[eV]***	**η_i *[%]***
^{40}Ca	Ta	2200-2800	81±1	−1.3±0.2	1.3×10^{-8} (2700)	0.9	Ta-TIS	-	-	-	4.9	3.4	15
	W	2300-2900	111±8	−0.6±0.7	2.6×10^{-10} (2700)	64	W-TIS	-	-	-	-	3.7	19
	Re	-	-	-	1×10^{-9} (2700)	12	Re-TIS	-	-	-	-	2.5	34
^{46}Ti	Ta	2300-2900	85±20	−2.1±1.8	1.3×10^{-9} (2700)	11	Ta-TIS	0.6	2	6.4	~ 5.6	5.4	0.8
	W	-	-	-	$\leq 8\times10^{-11}$ (2700)	>240	W-TIS	-	-	-	-	5.8	1.2
	Re	-	-	-	1.1×10^{-10} (2700)	120	Re-TIS	-	-	-	-	7.0	5.6
^{51}V	Ta	-	-	-	8×10^{-10} (2700)	12	Ta-TIS	0.4	1.4	6.3	~ 5.9	5.9	0.4
	W	-	-	-	8×10^{-11} (2700)	120	W-TIS	< 0.1	< 0.4	-	-	5.9	1.1
	Re	-	-	-	6×10^{-11} (2700)	150	Re-TIS	0.5	2	-	-	6.6	2.5
^{58}Ni	C2-23	-	-	-	1.1×10^{-11} (2400) - ≥50%	90	FEB-E2	-	-	-	-	-	>12
^{70}Zn	C	-	-	-	8.4×10^{-7} (2200) - >80%	0.03	FEB-B2	0.026*	-	-	-	-	>24
	C4-9	2200-2300	(109)	(2.07)	5×10^{-9} (2300)	0.8	FEB-B2	0.026*	-	-	-	-	31
	Nb	-	-	-	3.2×10^{-9} (2200)	4	FEB-B2	0.026*	-	-	-	-	28
	Ta	-	-	-	1.5×10^{-9} (2300)	6	FEB-B2	0.026*	-	-	2.2	2.3	30
^{84}Kr	C	-	-	-	3×10^{-8} (2200) - >50%	0.7	FEB-B2	0.028*	-	-	-	-	>30
	C4-9	-	-	-	1×10^{-10} (2300) - >50%	40	FEB-B2	0.028*	-	-	-	-	>30
^{120}Sn	C2-23	2200-2400	(60.6)	(−4.4)	1.3×10^{-10} (2400)	8	FEB-E2	1.4	-	-	~ 5.4	-	48
^{121}Sb	C2-23	2200-2400	(63)	(−5.4)	8×10^{-12} (2400)	120	FEB-E2	7	-	-	~ 5.2	-	>46
	C4-9	2200-2400	(83)	(−2.9)	3.6×10^{-11} (2400)	110	FEB-E4	3	-	-	~ 5.2	-	>30
	Ta	2200-2400	(79.3)	(−2.33)	3×10^{-10} (2400)	33	FEB-E4	3.3	-	-	-	-	>38
^{129}Xe	C	-	-	-	2.0×10^{-8} (2300) - >70%	1	FEB-B2	0.034*	-	-	-	-	>45
	C2-23	-	-	-	3.2×10^{-11} (2300) - ≥33%	32	FEB-B2	0.034*	-	-	-	-	>25
	C2-23	-	-	-	1×10^{-11} (2300) - ≥50%	100	FEB-E2	0.008*	-	-	-	-	>43
^{163}Dy	Ta	-	-	-	$<6\times10^{-11}$ (2300)	>150	FEB-H	1.9	2.4	5.5	-	5.0	>6.7
	Ta	-	46±2.7	−4.0	1.8×10^{-8} (2700)	-	[3]	-	-	-	-	-	-
	Ta	2200-2800	97.6±5.4	−0.17±0.47	9.1×10^{-9} (2700)	1	Ta-TIS	-	-	5.6	-	5.0	23
	W	2200-2900	102.2±11.6	−1.28±0.96	2.8×10^{-10} (2700)	33	W-TIS	-	-	-	-	5.5	28
	Re	2200-2900	122±6	0.7±0.5	6.8×10^{-10} (2700)	13	Re-TIS	0.055	0.2	-	-	5.0	48
^{208}Pb	C	-	-	-	5×10^{-8} (2200) - ≥80%	0.6	FEB-B2	0.043*	-	-	-	-	54
	C2-23	-	-	-	5×10^{-10} (2300)	2	FEB-E2	<0.03	-	-	~ 3.6	-	62
	C4-9	-	-	-	1.4×10^{-10} (2300) - >80%	30	FEB-B2	0.043*	-	-	-	-	>46

Table 2

Data on the formation of various molecular ions for a CF_4-flow of around 3×10^{-6} std.cm^3/s into the ion source. Thermoionization is performed in a high temperature cavity source with tantalum walls (see inset in fig.4), electron impact ionization in a FEBIAD-H ion source [6]. W_i is the ionization potential of molecule [15] or atom, respectively. τ_a is the mean surface sticking time per collision with a tantalum surface at 2300K, error estimated to be within a factor of 2. The τ_a values are with CF_4 addition for XF^+, and without for X^+.

	Ratio of ion currents		W_i	τ_a
	Thermo-ionization (Ta, 2300K)	Ionization by 150 eV electrons	[eV]	[μs]
NaF/Na	$< 10^{-5}$	$< 10^{-3}$	– / 5.14	– /0.04
KF/K	$< 10^{-6}$	$< 6\times10^{-6}$	– / 4.34	– /0.07
RbF/Rb	$< 5\times10^{-4}$	$< 4\times10^{-3}$	– / 4.18	– /0.1
CsF/Cs	$< 2\times10^{-6}$	$< 7\times10^{-6}$	8.8/ 3.89	– /0.2
BaO/Ba	$< 5\times10^{-5}$	—	6.9/ 5.21	– /6000
BeF/Be	—	50	9.1/ 9.32	0.6/200
MgF/Mg	—	3	7.8/ 7.64	<0.1/0.3
CaF/Ca	1.5	9±3 [a]	5.8/ 6.11	20/100
SrF/Sr	2.5	2	4.9/ 5.69	50/400
BaF/Ba	20	20	4.9/ 5.21	50/6000
BF/B	—	4	11.1/ 8.3	$0.4/>10^4$
AlF/Al	6×10^{-4} [b]	4	9.8/ 5.98	<0.1/600

[a] Uncertainty due to background of ^{40}Ar and ^{59}Co.

[b] Low ratio reflects the low thermoionization efficiency for AlF.

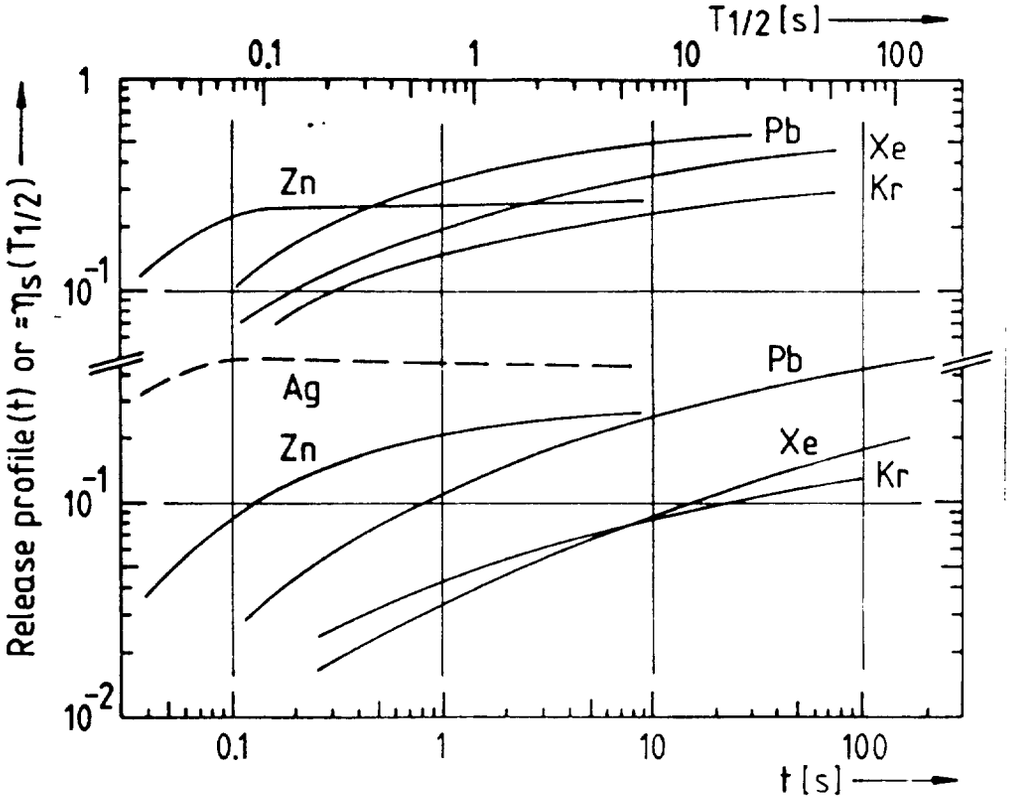

Fig. 1. Release profiles, i.e. fractions released within time t, for various volatile elements from graphite catchers in FEBIAD-B2-C [5] ion sources. The curves may alternatively be interpreted as approximately correct [1] halflife-dependent separation efficiencies using the $T_{1/2}$-scale. *Upper set of plots:* 5 µm thick carbon foil catchers at 2200 K. *Lower set:* catchers of 0.1 - 0.2 mm thick sintergraphite disks at 2300 K; average grain size ≤ 4 µm (manufacturer's data); tracer implantation about homogeneous in the top layer of grains; broken line: re-analyzed release of silver [1].

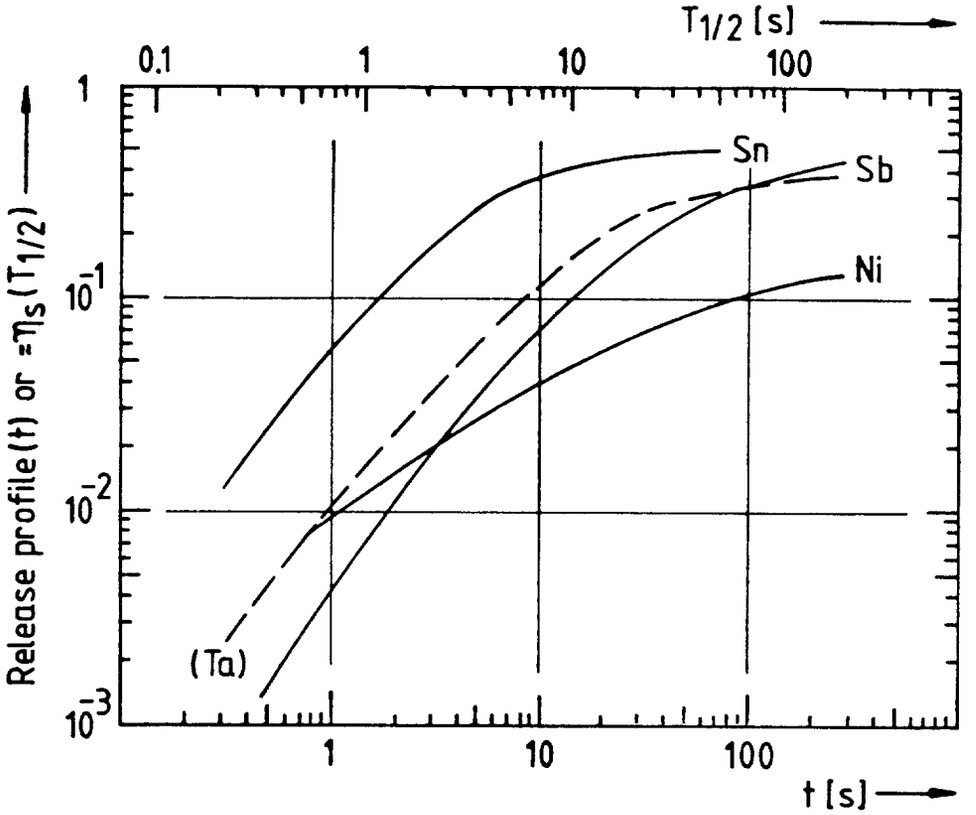

Fig. 2. Release profiles of various relatively refractory elements from FEBIAD-E ion sources [4], catcher temperature 2400 K. Solid lines for sintergraphite catchers, broken line 3 μm Ta catcher. The latter measurement is mainly interesting with respect to the considerably faster desorption part of the release which is due to a coating of the inner surfaces of the ion source with pyrolytic graphite here.

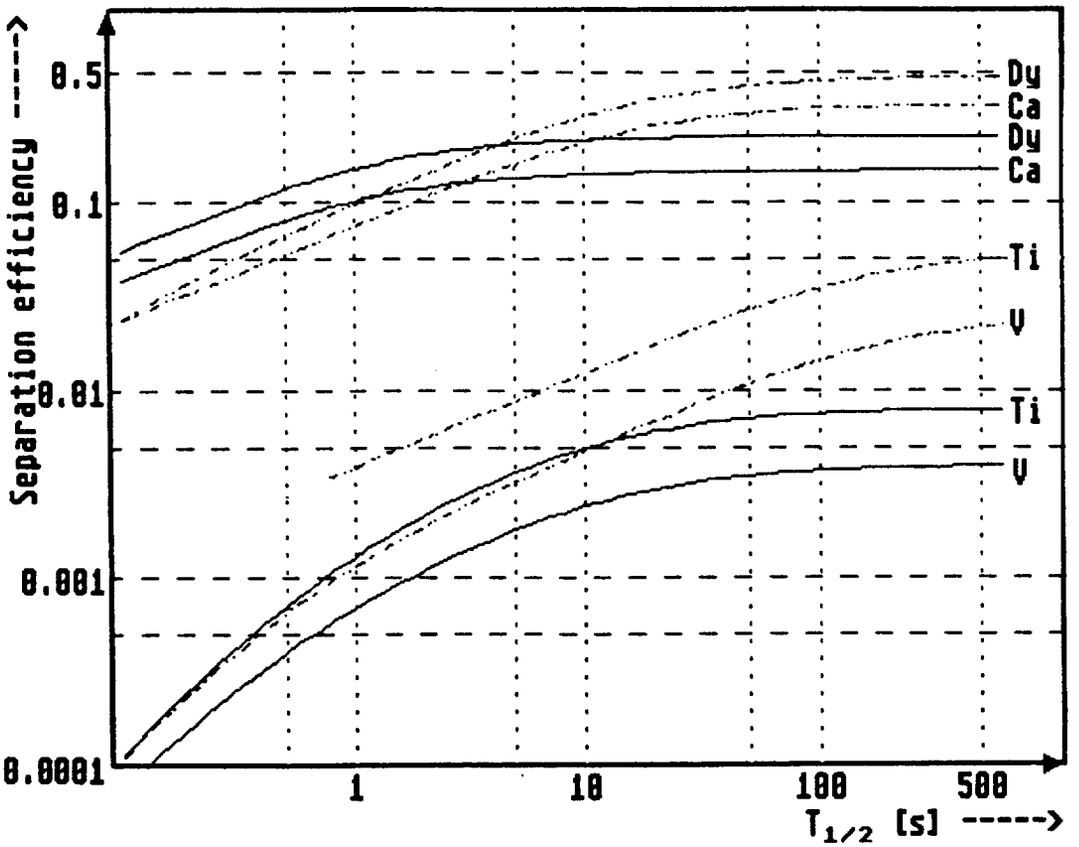

Fig. 3. Halflife-dependence of the separation efficiency of various tracers from 3 μm foil catchers in high temperature cavity ion sources [4] at 2700 K. Solid lines: Ta catchers in Ta cavities; broken lines: Re catchers in Re-lined tungsten cavities.

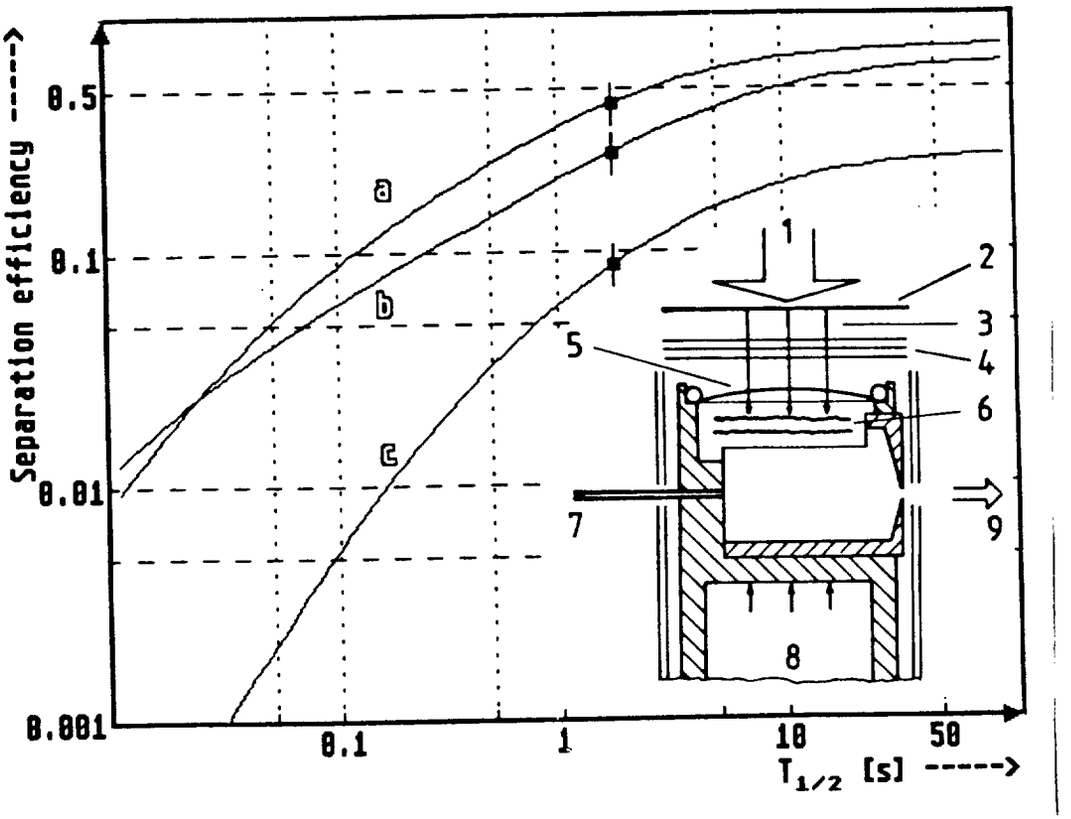

Fig. 4. Calculated halflife-dependence of the separation efficiency for barium from thin tantalum catchers in cavity-type thermo-ionizers. (a) for Ba^+ at 2700 K in the standard cavity [4]; (b) for BaF^+ in a special cavity with adequate CF_4 addition (see inset) at 2400 K, the "chemical evaporation" of the catchers preventing higher temperatures; (c) dito for Ba^+, the CF_4 flow being switched off. Points with error bars are based on the separation rates for ^{117}Ba ($T_{1/2}$ = 1.75 s) measured on-line as metal- or fluoride-ions in the $^{63}Cu(^{58}Ni, p3n)$ reaction and enable the "efficiency-calibration" of curves (b) and (c) versus (a). Inset: (1) UNILAC beam, (2) target, (3) reaction products, (4) heat shields, (5) entrance window, (6) tantalum catchers, (7) CF_4 and test vapour inlet, (8) electron bombardment heating, (9) separator beam.